Supplementary Information

Can magneto-plasmonic nanohybrids efficiently combine photothermia with magnetic hyperthermia?

Ana Espinosa,[a] Mathieu Bugnet,[b] Guillaume Radtke,[c] Sophie Neveu,[d] Gianluigi A. Botton,[b] Claire Wilhelm*‡[a] and Ali Abou-Hassan*‡[d]

Experimental Details

1. Chemicals.

The following chemicals were used in the experiments: Iron(II) chloride tetrahydrate ($FeCl_2.4H_2O$; 99%), iron(III) nitrate nonahydrate ($Fe(NO_3)_3.9H_2O$; 98%), sodium hydroxide (NaOH; 99.99%), diethylene glycol (DEG; 99%), N-methyldiethanolamine (NMDEA; 99%), sodium citrate tribasic dihydrate (98%), nitric acid (HNO_3; 70%), N, N-dimethylformamide (DMF), poly(vinylpyrrolidone) (PVP; MW 10 000), $NaBH_4$, gold (III) chloride hydrate ($HAuCl_4.xH_2O$; 99.999%), ammonium hydroxide solution (20%) and ethanol. All chemicals were purchased from Sigma-Aldrich (France) except Iron(II) chloride tetrahydrate ($FeCl_2.4H_2O$; 99%), ethanol, acetone, and ethyl acetate were obtained from VWR (France). All aqueous solutions were prepared using Millipore water (resistivity 18.2 MΩ).

2. Synthesis of magnetoplasmonic nanoparticles.

2.1. Maghemite multi-core nanoparticles (MagNPs) synthesis.

First, 1.082 g (4 mmol) of $FeCl_3.6H_2O$ and 0.398 g (2 mmol) $FeCl_2.4H_2O$ were completely dissolved in 80 g of liquid mixture of NMDEA and DEG with 1:1 (v/v) ratio. The solution was stirred for 1 h. Separately; 0.64 g (16 mmol) of NaOH was dissolved in 40 g of polyols. This solution was added to the solution of iron chlorides, and the resulting mixture was stirred for another 3 h. Then, the temperature was elevated to 220°C using a progressive heating of 2°C/min. Once the temperature reached 220°C, the solution was stirred for 12 h. The black precipitate was separated magnetically and washed with mixture of ethanol and ethyl acetate (1:1, v/v) several times to eliminate organic and inorganic impurities. Possible iron hydroxides were removed by treatment with 10% nitric acid.

Then, 8.25 g of iron(III) nitrate was dissolved in 20 mL water and added to the nanoparticles. The resulting mixture was heated to 80°C for 45 min to achieve a complete oxidation of the nanoparticles. After another treatment with 10 % nitric acid, the particles were washed twice with acetone and diethyl ether and dispersed in water; multi-core MagNPs were obtained. The iron content of the sample was titrated using flame atomic absorption spectroscopy.

2.2. Seeding the surface of MagNPs with gold (MagNP-seeds).

In order to deposit seeds on the surface of the MagNPs, their surface was functionalized with citrate anions. The MagNP suspension was heated at 80°C and citrate ions were added to the suspension with a molar ratio of citrate/iron = 0.2. The mixture was heated at 80°C for 30 min than precipitated with acetone, washed with diethyl ether and dispersed in water. The iron content of the sample was titrated using flame atomic absorption spectroscopy.

Under vigorous stirring, in 100 ml of Millipore water alkalinised with ammonia (pH = 10), 5 mg of citrate treated MagNPs and 680 µl of a 35 mM $HAuCl_4$ aqueous solution were mixed. The mixture was heated at 40°C for 15 minutes, followed by magnetic separation and redispersion of the NPs in 100 ml of water.

1 ml of a freshly prepared 0.1 M $NaBH_4$ solution was added to the previous suspension under vigorous stirring. Nanoparticles were magnetically separated and washed three times with water. Finally the NPs were redispersed in a 100 mL solution of PVP (10 mM) in ethanol.

2.3. Growth of magneto-plasmonic nanoparticles (MagPlasNPs).

Under vigorous stirring, 1.13 mL of 50 mM $HAuCl_4$ aqueous solution was added to 100 ml of a 10 mM PVP solution in DMF. After 10 minutes (time needed to reduce the Au^{3+} to Au^{+}, see for more details[1]) x ml (x = 7; 13; 20) of the previously prepared MagNP-seeds dispersion in ethanol was added under constant stirring. The colour of the solution turned blue after 30 minutes, the magnetic particles were separated with a magnet, washed by centrifugation (7000 rpm, 20 min) twice with ethanol to remove excess PVP and DMF, once with Millipore water and finally redispersed in 1 mL of Millipore water.

3. Characterizations.

Conventional transmission electron microscopy (TEM).

All TEM images were obtained by using a JEOL 100 CX instrument (100 kV).

Elemental analysis.

The concentrations of the iron and gold content were measured by elemental analysis using an ICP-AES spectrometer (iCAP 6500, Thermo). The samples were digested in concentrated HNO_3 and HCl solution.

UV-Vis-NIR spectroscopy.

Optical spectra were obtained using Avaspec-USB2 UV-VIS-NIR Spectrometer.

Dynamic Light Scattering (DLS) and nanoparticle tracking analysis (NTA).

Size distributions were obtained using NanoSizer and Nanosight instruments (Malvern Instrument).

Scanning transmission electron microscopy (STEM): chemical and surface plasmonic mapping.

The nanoparticles were diluted in HPLC-grade methanol, ultrasonicated, and a drop of the solution was deposited onto an ultrathin carbon film on a holey carbon support grid (Ted Pella Inc.). Chemical maps were acquired in Electron Energy Loss Spectroscopy (EELS) using the Spectrum Imaging technique in Scanning Transmission Electron Microscopy (STEM) on a FEI Titan Cubed 80-300, operated at 200 kV, equipped with a Gatan GIF Quantum electron energy loss spectrometer, and with spherical aberration correctors of the probe and image lenses. Spectrum Images (SI) were recorded with a dispersion of 1eV/channel ensuring the simultaneous acquisition of the O-K (~530 eV), the Fe-L_{23} (~708 eV) and the Au-M_{45} (~2206 eV) edges. Elemental maps were obtained by fitting the background in the pre-edge region using a power-law model and integrating the signal over a 70 eV energy window starting at the edge onset for each of these three edges. Principal component analysis was employed to filter the raw data to reduce the channel-to-channel noise.

The surface plasmon maps were obtained in STEM on an image corrected FEI Titan 80-300, operated at 80 kV, and equipped with a monochromator and a Gatan GIF Tridiem EELS spectrometer. The energy resolution was 70 meV as given by the FWHM of the elastic peak, and a dispersion of 0.01 eV/channel was used. Surface plasmon maps were obtained by first aligning all individual spectra in energy, subtracting the zero-loss peak using the reflected tail model, and integrating the signal over the 1.4-2.4 eV energy range.

Magnetic properties analysis.

Magnetic and magneto-plasmonic nanoparticles suspensions were introduced in sample holding capsules for Vibrating Sample Magnetometer analysis (VSM, PPMS, Quantum Design, Inc.). Field-dependent magnetization curves were measured at room temperature as a function of the external field in the range of 0-0.5 T.

Magnetic hyperthermia measurements.

Two magnetic hyperthermia applicator were used. A home-made coil was used to deliver a magnetic field at 900 kHz and 25 mT, in order to optimize the magnetic heating efficiency. A volume of 100 µL of aqueous solution (MagNPs and/or MagPlasNPs) was then inserted in a small eppendorf tube was placed inside the coil (1.8 cm of diameter). The temperature inside the sample holder was kept constant at physiological conditions (37°C) by circulating nonane into the coil circuit. An infrared thermal imaging camera (FLIR SC7000) was used to measure the increase in temperature. The camera was placed at the opposite end of the sample holder cavity (coil), collecting the cross sectional view of the bottom of the sample. The second coil used (5 cm diameter, inductive heater, Nanotherics, Corp) delivers an AC magnetic field of 25 mT at a frequency of 110 kHz (within the safe limit for tissue exposure), and was used for temperature measurements both in solution and *in vivo*.

All reported temperature curves and values were calculated after collecting at least three experimental measurements.

Photothermal measurements.

A 680 nm and 808 nm-laser diode coupled to an optic fiber were used to activate photothermal effect on samples (Laser Components S.A.S, (France)) with an adjustable power up to 5 W. The same sample holder was used for both magnetic hyperthermia and photothermal effect measurements. This configuration has two goals: using the same cooling circuit to thermalize the sample at 37°C as initial temperature and applying combined hyperthermia (using simultaneous magnetic induction). The distance between sample and laser was 2-3 cm with a spot of 1 cm^2 and power laser was tuned between 0.10 and 0.5 W/cm^2. Temperature elevation was recorded using the same infrared thermal imaging camera (FLIR SC7000) in the same configuration.

***In vitro* cell uptake experiments**.

Human prostate adenocarcinoma, (PC3 cell line) was cultured in DMEM medium supplemented with 10% FBS and 1% penicillin in 150 cm^3 flasks under 5% CO_2 atmosphere.

Cells were incubated at 37°C with magnetic nanoparticles (MagNP) at [Fe] = 0.4 mM for 30 min in 5%-citrated RPMI medium and with magneto-plasmonic particles (MagPlasNP-1 and MagPlasNP-2) at [Fe] = 0.03 mM overnight in DMEM medium.

Heating efficiency *in vivo*.

In vivo experiments were performed in agreement with guidelines on animal care and use of Animalerie Buffon (Institute Jacques Monod, Paris 7). Studies on tumour bearing mice were carried out in 9 week old male immunodeficient athymic nude NMRI mice, with the mean weight of 30 g provided by Janvier (France).

Each mouse was subcutaneously injected in the left and right flank with 20×10^6 PC3 cells suspended in 100 µL of PBS. When the tumours were grown to a diameter of 5-7 mm, the mice were intratumorally injected with 100 µL of MagPlasNPs solution ([Fe] = 150 mM) of iron concentration suspended in physiological saline medium (PBS). The animal was anesthetized with a ketamine/xylazine solution and was placed into a 5 cm diameter coil of the inductive heater (Nanotherics, Corp) and immediately exposed to hyperthermia treatment: AC magnetic field (110 kHz, 25 mT) or/and laser irradiation (680 nm, 0.3 W/cm^2).

The infrared thermal camera FLIR SC7000 (FLIR Systems, Inc.) was used to monitor the superficial temperature of tumours of mice.

Transmission electron microscopy (TEM) and histology of tumours.

After excision, tumours were cut into 1 mm^3 pieces and fixed with 2% glutaraldehyde in 0.1 M sodium cacodylate buffer, postfixed with 1% osmium tetroxide containing 1.5% potassium cyanoferrate, gradually dehydrated in ethanol and embedded in Epon. Thin sections (70 nm) of selected zones were observed with JEOL 100 CX instrument (100 kV). For histology analysis, tumors were fixed with phosphate-buffered 10% formalin at pH 7.4, dehydrated in graded ethanol solutions and embedded in paraffin. Six-micrometer-thick sections were stained with Prussian Blue (Perls) for optical microscopy observation.

Supplementary Figures

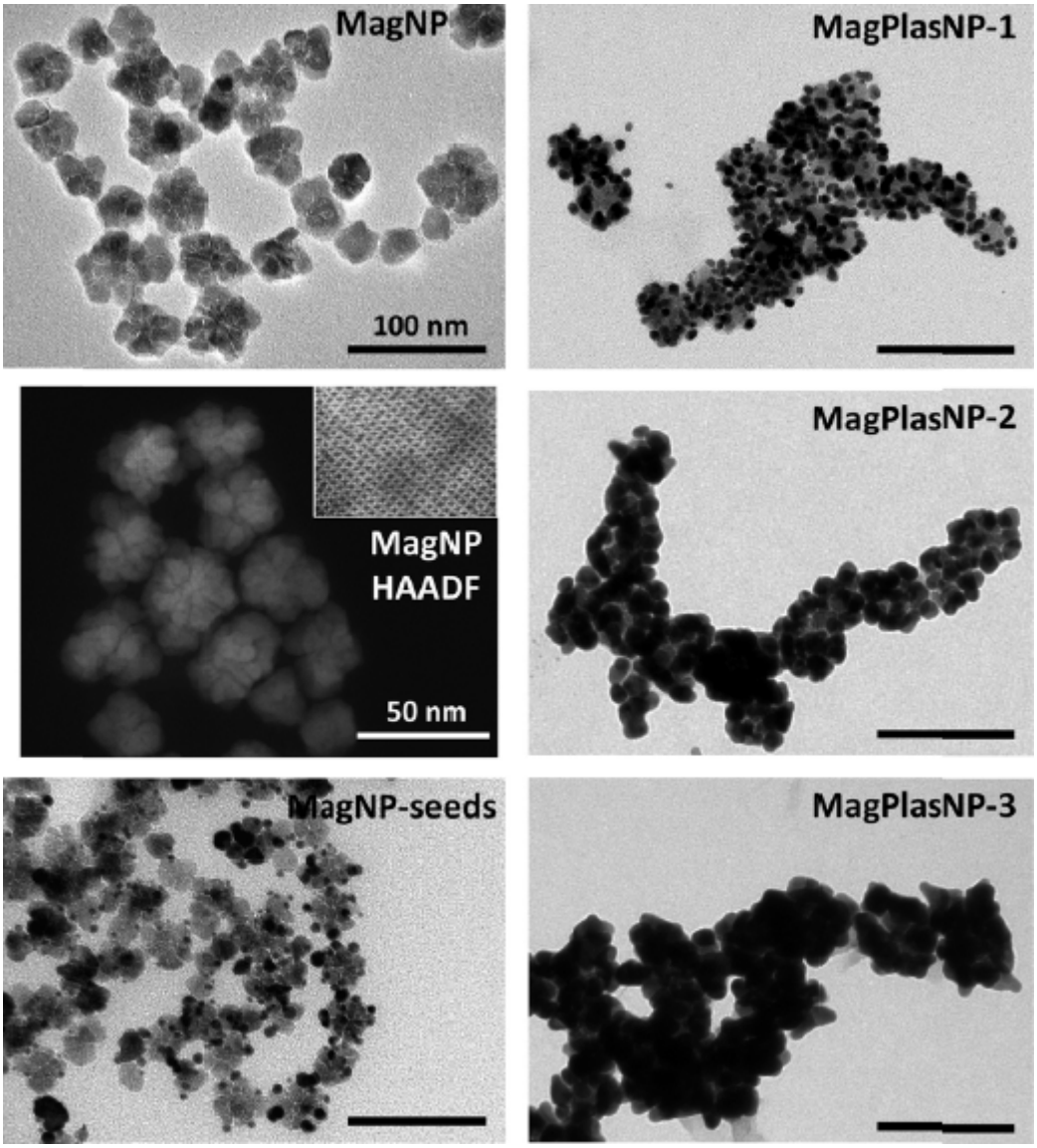

Fig. S1. **TEM images of all nanostructures**. Bare multi-core maghemite nanoparticles (MagNP), MagNPs decorated with Au seeds (MagNP-seeds), and magneto-plasmonic nanohybrids with different Au/Fe ratio (MagPlasNP-1, 2 and 3) are shown. For MagNP, the HAADF image is also presented, with a high-resolution, atomic resolved image, of maghemite in inset.

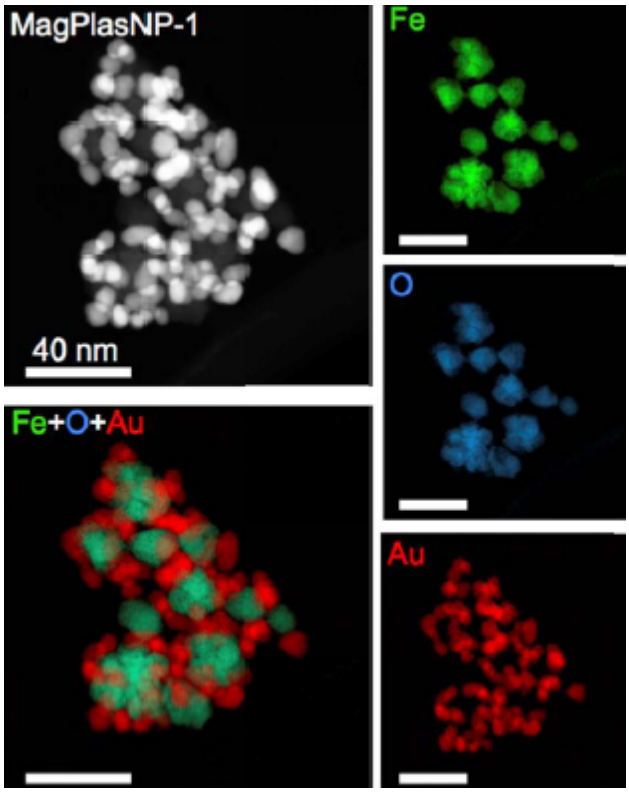

Fig. S2: Elemental analysis of different MagPlasNP-1. HAADF image, EELS Fe map (green), EELS O map (blue), EELS Au map (red) and overlaid maps.

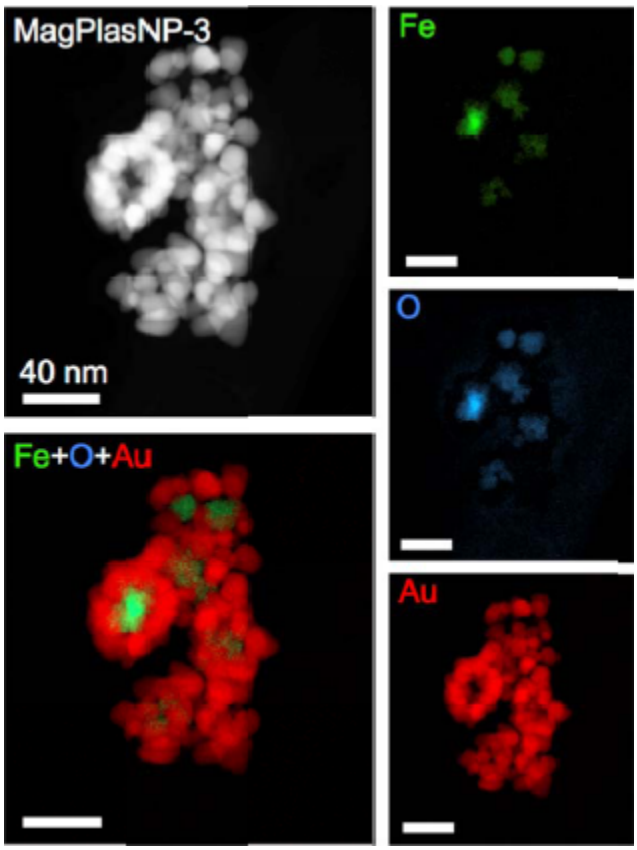

Fig. S3: Elemental analysis of different MagPlasNP-3. HAADF image, EELS Fe map (green), EELS O map (blue), EELS Au map (red) and overlaid maps.

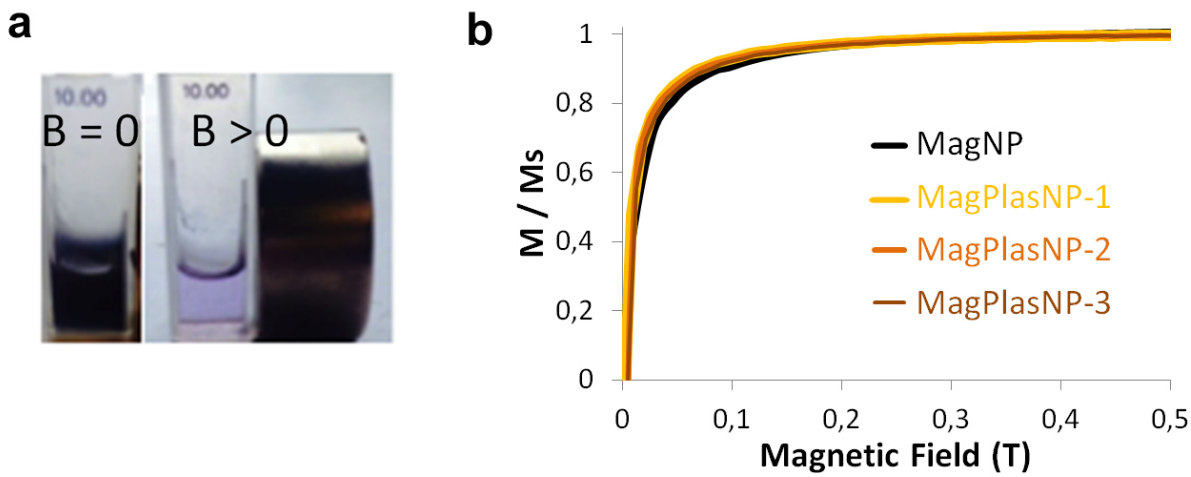

Fig. S4. **Superparamagnetic behavior of the nanohybrid**. (a): Attraction of MagPlasNP-2 by a permanent magnet. (b): Magnetization curves of MagNP and MagPlasNP-1,2, and 3.

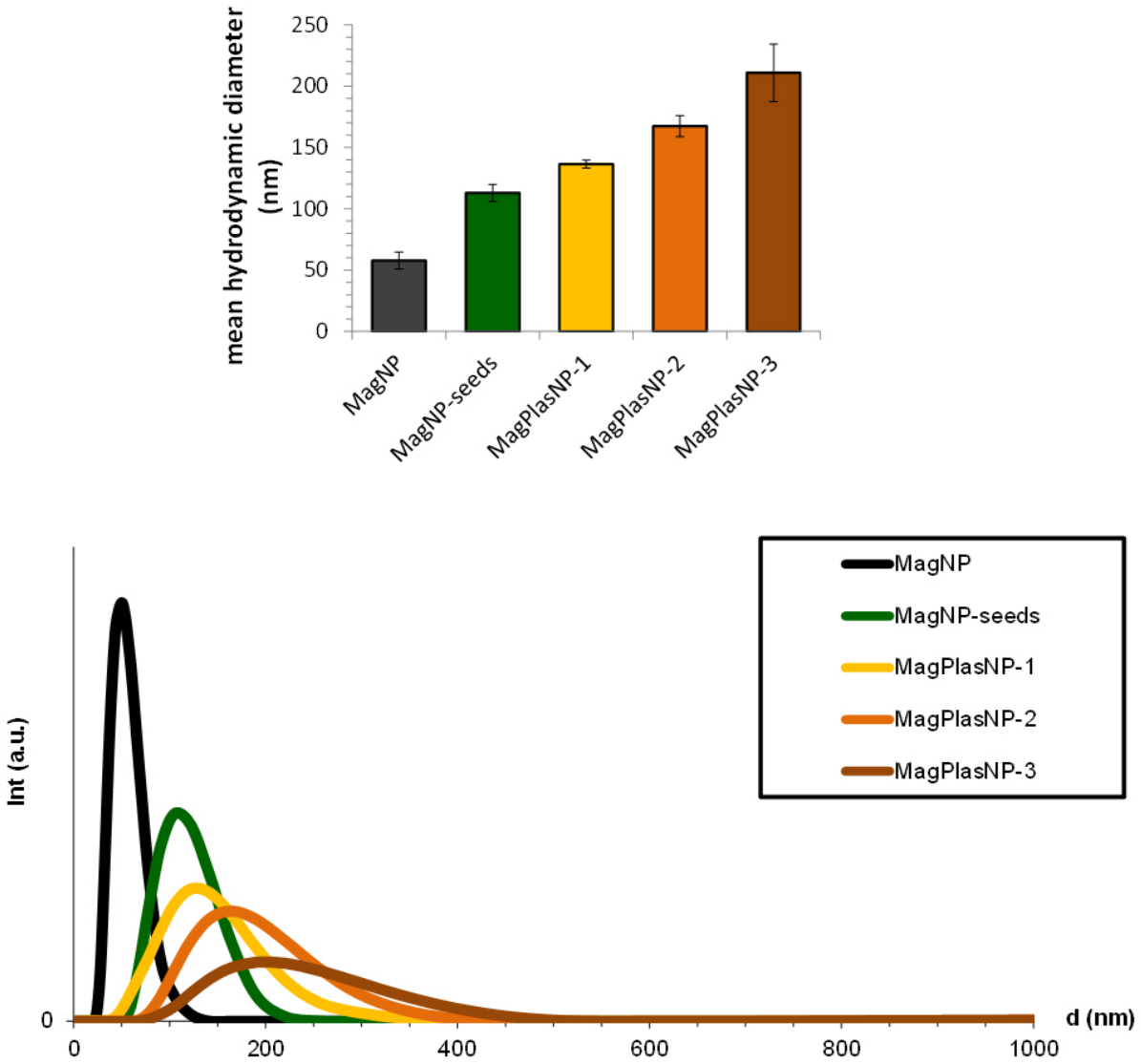

Fig. S5. Stability of the nanohybrids evidenced by dynamic light scattering (DLS) measurements in water. Top: Average hydrodynamic diameter (nm) of magnetic nanoparticles (MagNPs), magnetic nanoparticles seeds (MagNP-seeds) and magneto-plasmonic nanoparticles (MagPlasNP-1, MagPlasNP-2 and MagPlasNP-3). **Bottom**: Typical size distribution curves.

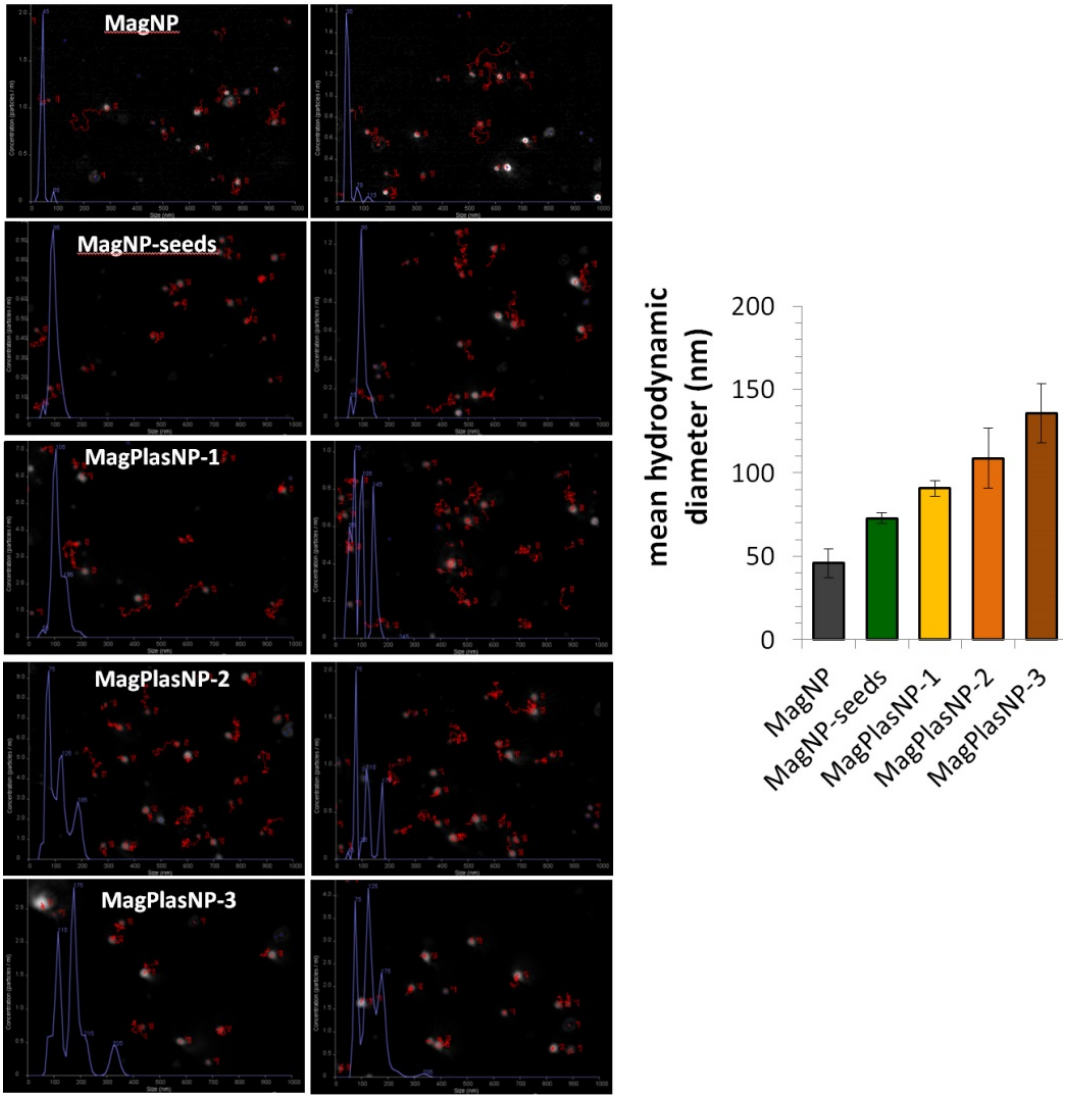

Fig. S6. Stability of nanohybrids dispersed in water evidenced by following their Brownian motions. Left: Typical trajectories (in red) recorded for magnetic nanoparticles (MagNPs), magnetic nanoparticles seeds (MagNP-seeds) and magneto-plasmonic nanoparticles (MagPlasNP-1, MagPlasNP-2 and MagPlasNP-3). From each trajectory, the diffusion coefficient is computed, and the diameter of the tracked nanoparticle can be derived from the Stokes Einstein equation. **Right**: 500 nanoparticles were tracked for each condition, and the corresponding average diameters are presented on the plot.

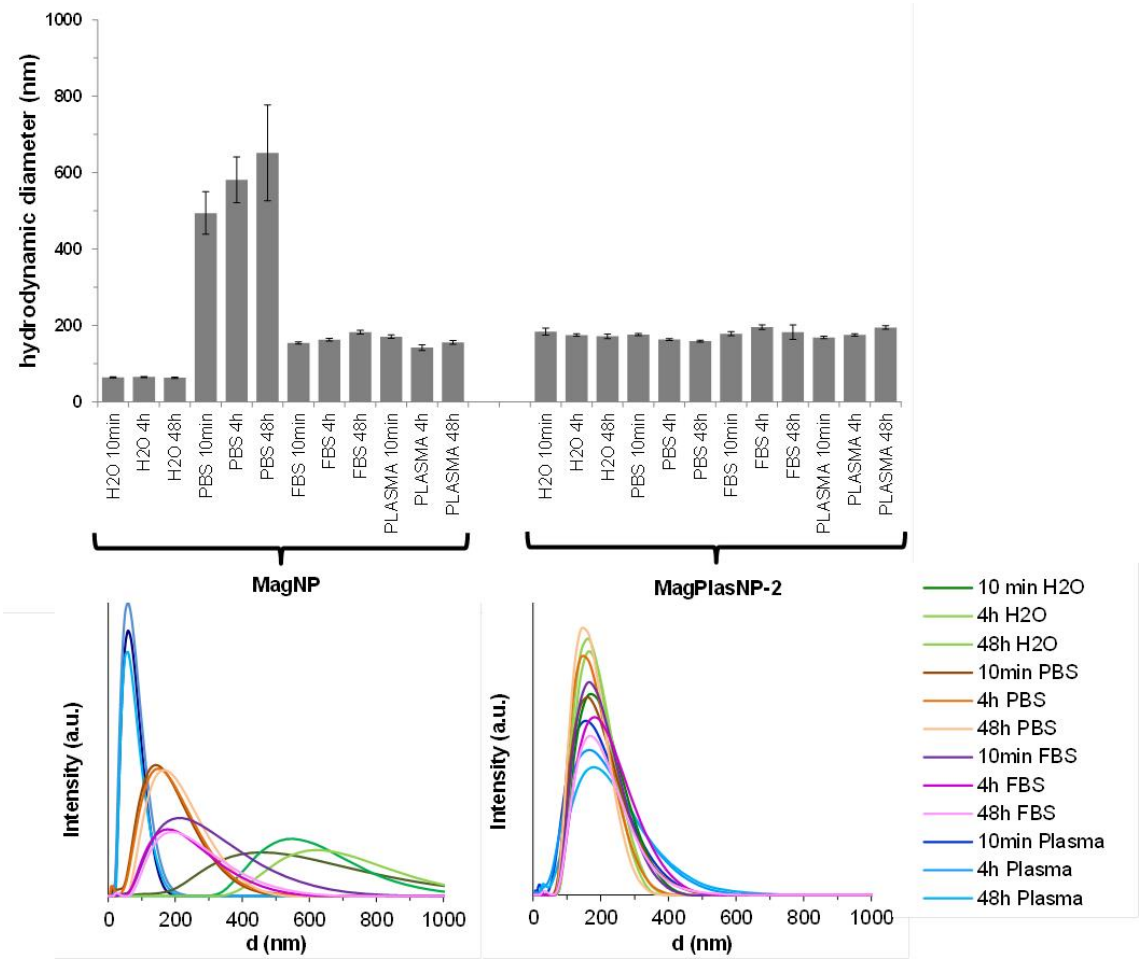

Fig. S7. Stability of the magnetic nanoparticles MagNP, and the magneto-plasmonic nanohybrids MagPlasNP-2 with time in different media. **Top**: Average hydrodynamic diameter (nm) of MagNP and MagPlasNP-2 dispersed in water, phosphate buffer solution (PBS), fetal bovine serum (FBS ; 20% of serum in cell culture medium) and plasma, measured after different times following their dispersion (after 10 min, 4h and 48h), by dynamic light scattering (DLS). **Bottom**: Typical size distributions for each time point and medium conditions.

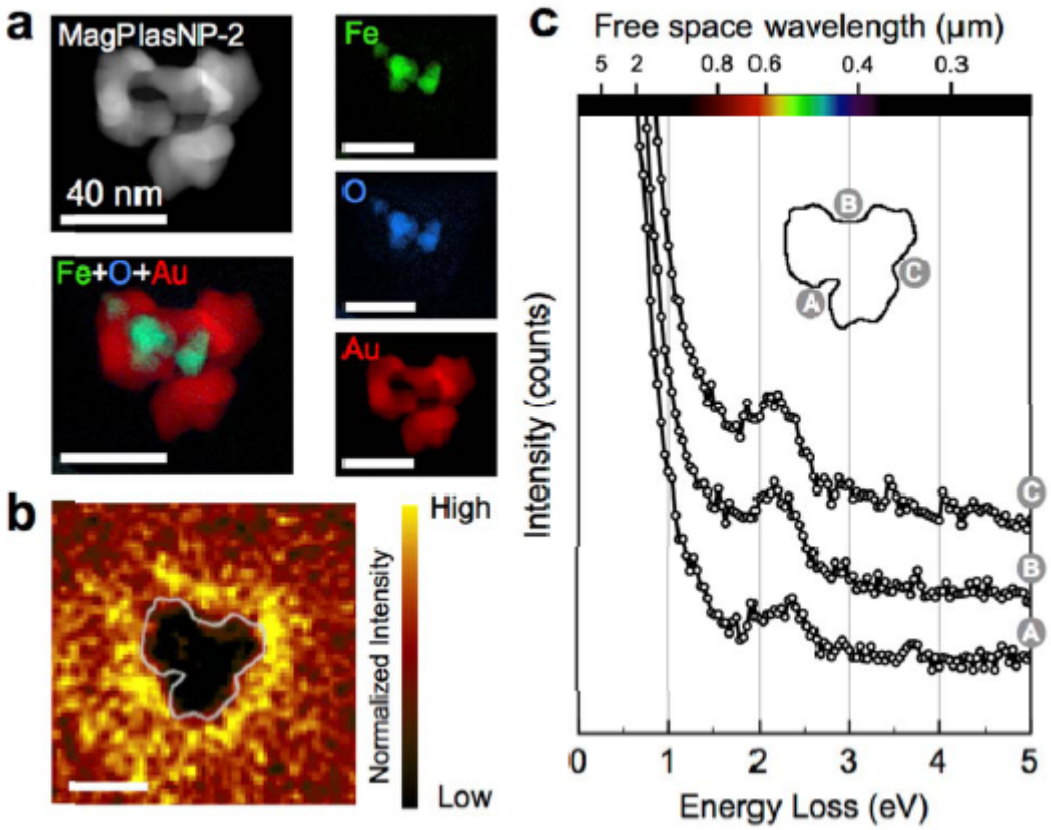

Fig. S8: Surface plasmon resonances and EELS elemental analysis of two MagPlasNP-2 hybrids. (a) HAADF image, EELS Fe map (green), EELS O map (blue), EELS Au map (red) and overlaid maps. (**b)** Surface plasmon resonance map (smoothed) corresponding to the 1.4-2.4 eV energy range. The contour of the nanohybrid is superimposed to the map. (**c)** Energy loss spectra corresponding to three different beam positions. A single broad resonance is observed at ~ 2.2 eV ($\lambda \sim 560$ nm). Raw data are shown.

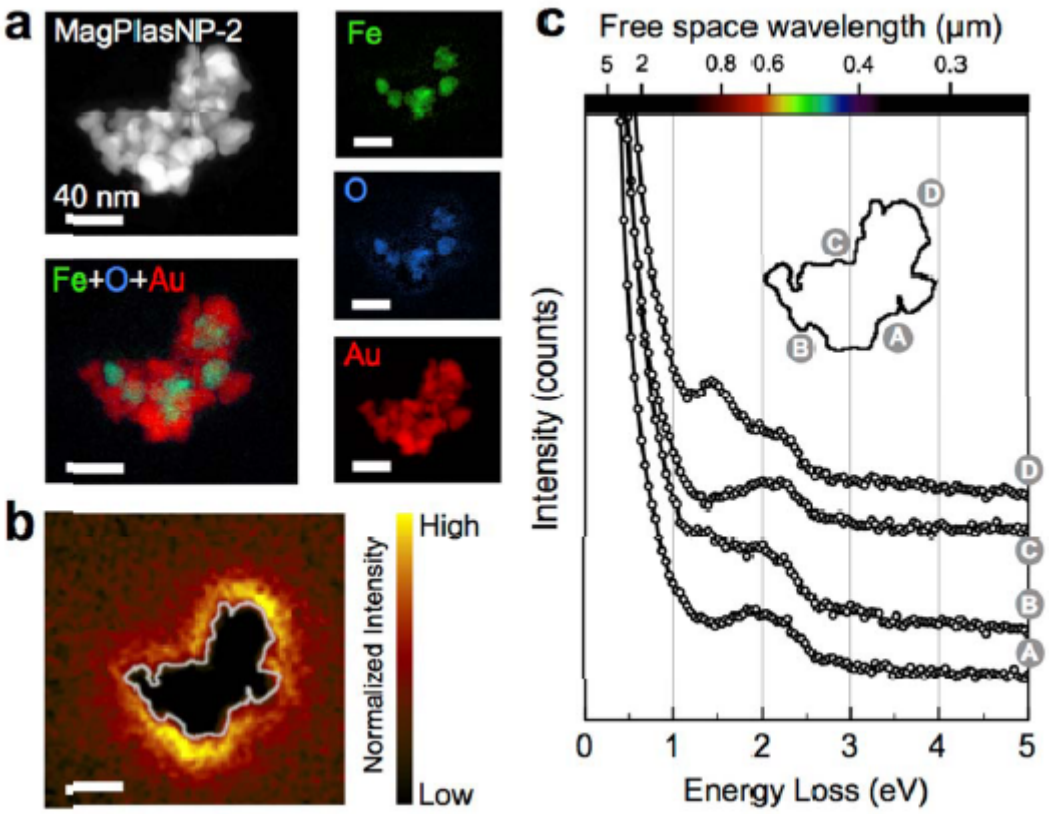

Fig. S9: Surface plasmon resonances and EELS elemental analysis of five MagPlasNP-2 hybrids. (a) HAADF image, EELS Fe map (green), EELS O map (blue), EELS Au map (red) and overlaid maps. (**b)** Surface plasmon resonance map (smoothed) corresponding to the 1.4-2.4 eV energy range. The contour of the nanohybrid is superimposed to the map. (**c)** Energy loss spectra corresponding to four different beam positions. Two distinct broad resonances at ~ 1.45 eV ($\lambda \sim 855$nm) and ~ 2.2 e V ($\lambda \sim 560$nm) can be identified depending on the spatial position of the electron beam. Raw data are shown.

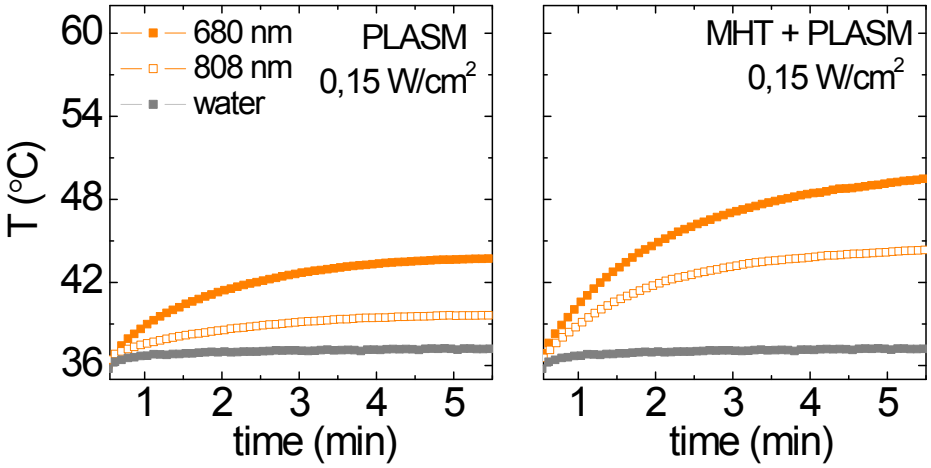

Fig. S10: Heating effect of nanohybrids using magnetic and plasmonic hyperthermia as a function of the excitation wavelength. Temperature elevation profiles of magneto-plasmonic nanoparticles (MagPlasNP-2) under photothermal irradiation (PLASM) using 680 and 808 nm laser (left) and the combination with magnetic induction (MHT + PLASM) (at 900 kHz and 25 mT) at 0.15 W/cm^2.

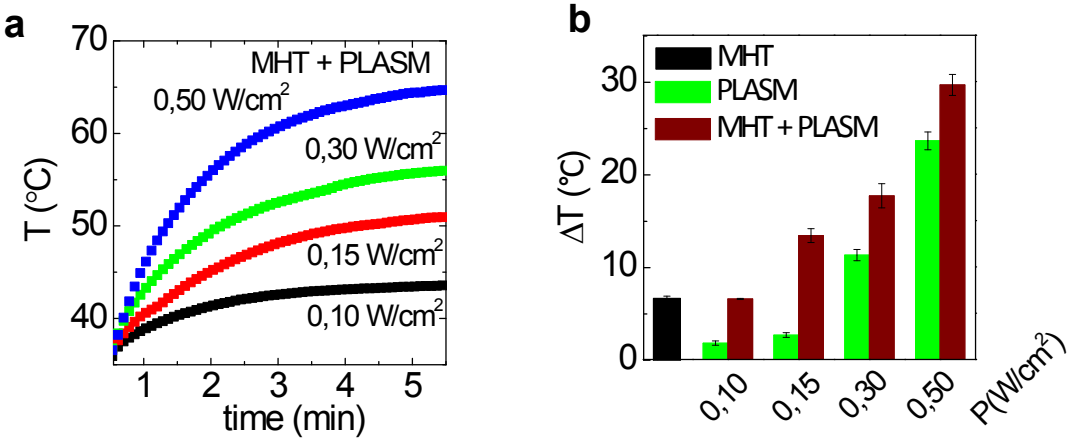

Fig. S11: Heating effect of nanohybrids using magnetic and plasmonic hyperthermia. (a) Temperatures reached after 5 min under application of both magnetic and plasmonic effect (MHT + PLASM) on MagPlasNP-2 at 0.1, 0.15, 0.3 and 0.5 W/cm^2 of power laser. **(b)** Temperatures obtained after 5 min on MagPlasNP-2 under a MHT + PLASM induction at 680 nm laser power density of 0.1, 0.15, 0.3 and 0.5 W/cm^2.

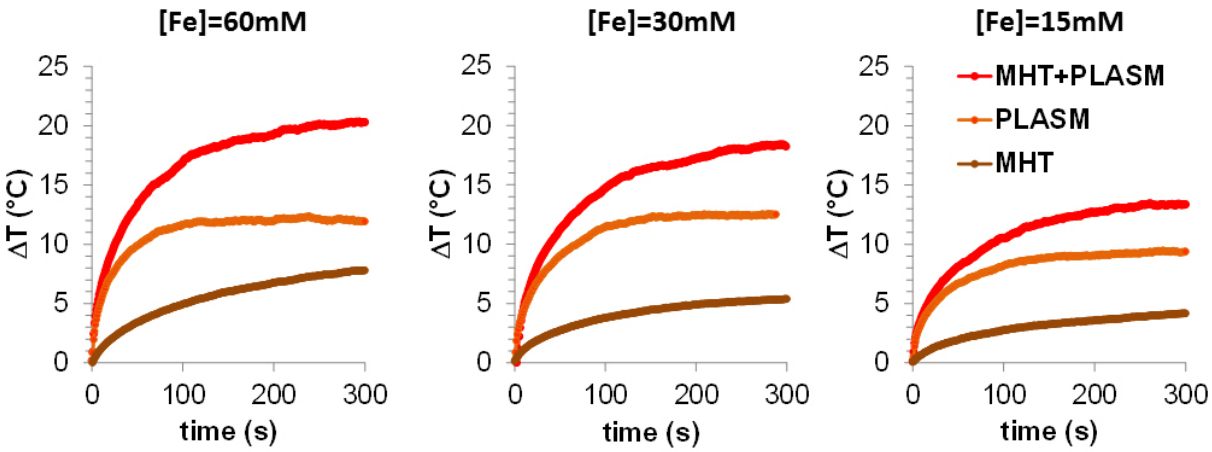

Fig. S12: Temperature profiles for MagPlasNP-2 at different concentrations ([Fe] = 60, 30 and 15 mM). Settings for magnetic hyperthermia (MHT): 110 kHz, 25 mT. Settings for laser (PLASM): 680 nm, 0.3 W/cm².

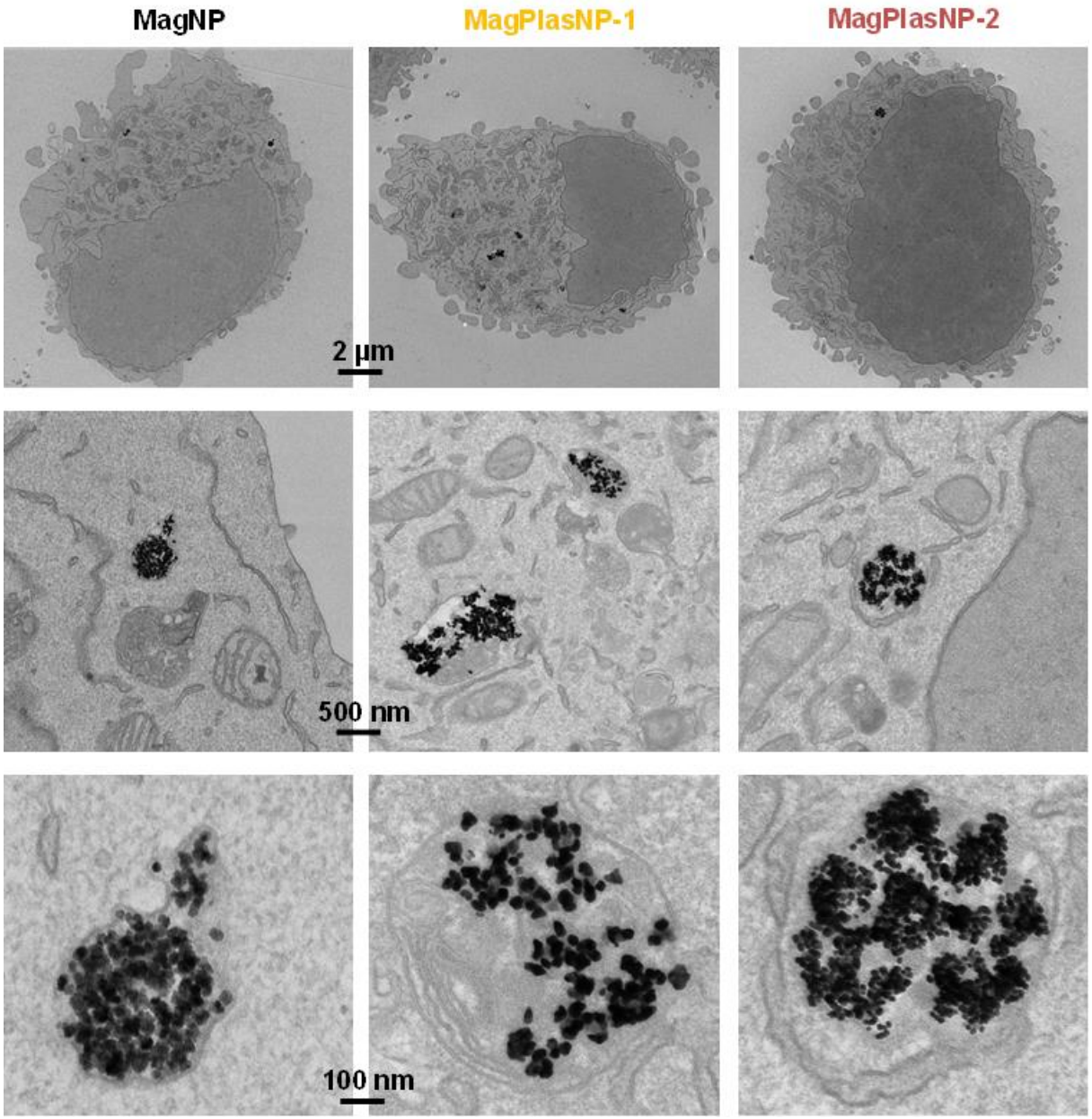

Fig. S13: *In vitro* cell uptake of nanohybrids. TEM images of PC3 cancer cells after incubation with magnetic nanoparticles (MagNP) (left) and magneto-plasmonic nanoparticles MagPlasNP-1 (center) and MagPlasNP-2 (right), showing intracellular endosomes at different magnifications.

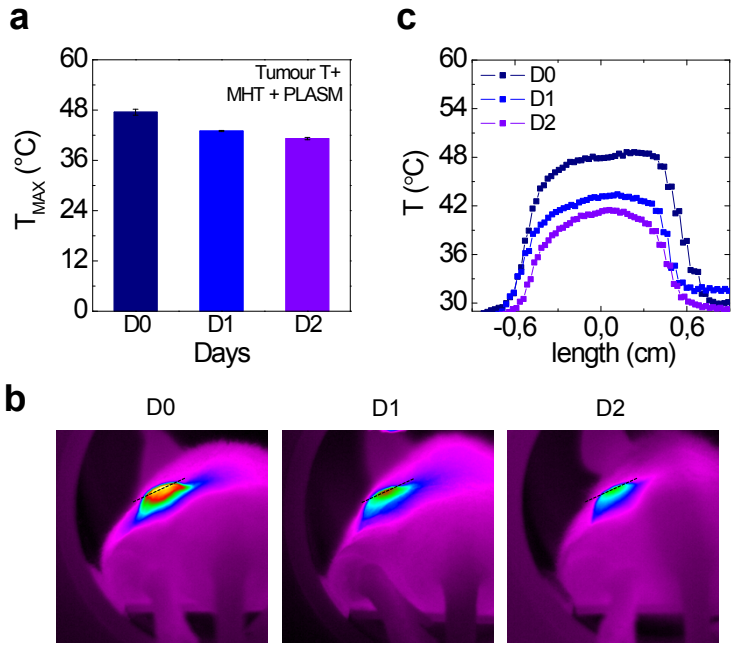

Fig. S14. Evolution and distribution of tumour temperature over post-injection time. (a) Maximum temperature raised in injected tumors recorded at day 0 (D0), day 1 (D1) and day 2 (D2) after MagPlasNP-2 injection. **(b,c)** Thermal images of the tumor during treatment at D0, D1 and D2 (b), and corresponding temperature distribution in the cross-section (c). Global heating is recorded in macroscopic centimeter zones.

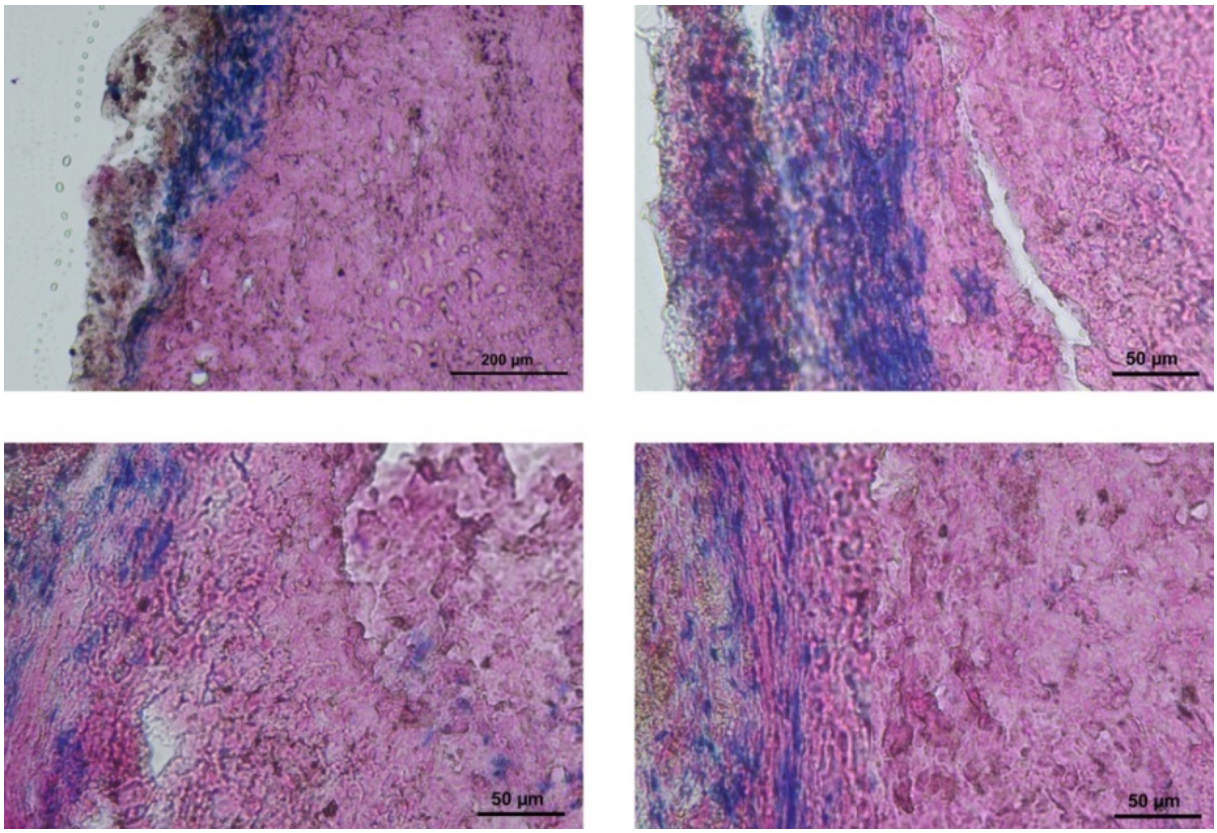

Fig. S15. Microstructure of nanohybrid-injected tumor. Histological micrographs of an injected tumor with MagPlasNP-2 after Prussian Blue staining (Perls) corresponding to different tumour regions.

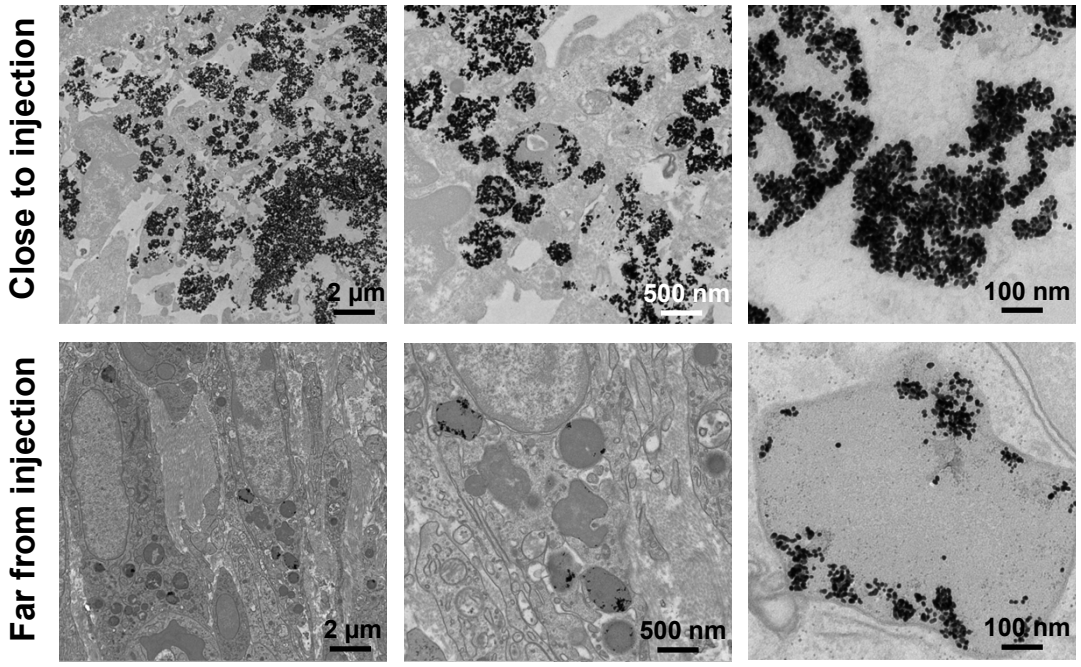

Fig. S16: Tumor injection of nanohybrids. TEM micrographs of tumours injected with MagPlasNP-2 nanohybrids in two regions: close (upper panel) and far (lower panel) to injection point at different magnifications, two days after injection.

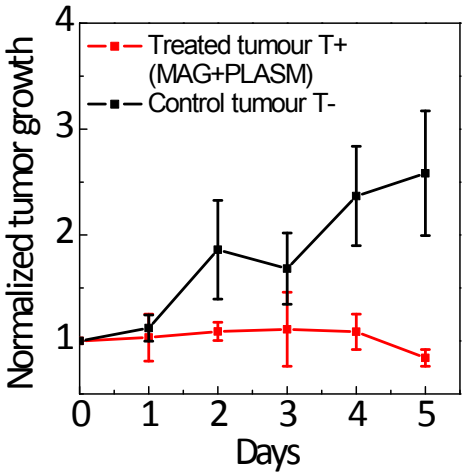

Fig. S17. Preliminary study of *in vivo* bimodal (MAG+PLASM) efficacy on tumor-bearing mice. Normalized average tumor growth (two tumors) for treated tumors (N=2) injected with MagPlasNP-2 and exposed to bimodal MAG+PLASM hyperthermia, compared to untreated tumors, over 5 days following the heating protocols.

References

1. S. Barbosa, A. Agrawal, L. Rodríguez-Lorenzo, I. Pastoriza-Santos, R. A. Alvarez-Puebla, A. Kornowski, H. Weller and L. M. Liz-Marzán, *Langmuir*, 2010, **26**, 14943-14950.